



CHORUS

This is the accepted manuscript made available via CHORUS. The article has been published as:

Absence of paired crossing in the positive parity bands of ^{124}Cs

A. K. Singh, A. Basu, Somnath Nag, H. Hübel, J. Domscheit, I. Ragnarsson, A. Al-Khatib, G. B. Hagemann, B. Herskind, D. R. Elema, J. N. Wilson, R. M. Clark, M. Cromaz, P. Fallon, A. Görgen, I.-Y. Lee, D. Ward, and W. C. Ma

Phys. Rev. C **97**, 024323 — Published 20 February 2018

DOI: [10.1103/PhysRevC.97.024323](https://doi.org/10.1103/PhysRevC.97.024323)

Absence of paired crossing in the positive parity bands of ^{124}Cs

A. K. Singh and A. Basu

Department of Physics, Indian Institute of Technology Kharagpur, Kharagpur - 721302, India

Somnath Nag*

Department of Physics, National Institute of Technology Raipur, GE Road, Raipur - 492010, India

H. Hübel and J. Domscheit

Helmholtz-Institut für Strahlen-und Kernphysik, Universität Bonn, Nussallee 14-16, D-53115 Bonn, Germany

I. Ragnarsson

Division of Mathematical Physics, LTH, Lund University, P.O. Box 118, SE-221 Lund, Sweden

A. Al-Khatib

Department of Physics, Faculty of Science, University of Damascus, Damascus, Syria

G. B. Hagemann, B. Herskind, D. R. Elema,[†] and J. N. Wilson[‡]
Niels Bohr Institute, Blegdamsvej 17, DK-2100 Copenhagen, Denmark

R. M. Clark, M. Cromaz, P. Fallon, A. Görgen,[§] I. -Y. Lee, and D. Ward
Nuclear Science Division, Lawrence Berkeley National Laboratory, Berkeley, California 94720, USA

W. C. Ma

Department of Physics, Mississippi State University, Mississippi State, Mississippi 39762, USA

High-spin states in ^{124}Cs were populated in the $^{64}\text{Ni}(^{64}\text{Ni}, p3n)$ reaction and the Gammasphere detector array was used to measure γ -ray coincidences. Both, positive and negative parity bands, including bands with chiral configurations, have been extended to higher spin, where a shape change has been observed. The configurations of the bands before and after the alignment are discussed within the framework of the cranked Nilsson-Strutinsky model. The calculations suggest that the nucleus undergoes a shape transition from triaxial to prolate around spin $I \simeq 22$ of the positive-parity states. The alignment gain of $8 \hbar$, observed in the positive-parity bands, is due to partial alignment of several valence nucleons. This indicates the absence of band crossing due to paired nucleons in the bands.

PACS numbers: 23.20.Lv, 23.20.En, 27.60.+j, 21.60.Ev

Keywords:

I. INTRODUCTION

The transitional nuclei in the mass-125 region are of considerable interest because of the competing shape-driving

tendencies of the $h_{11/2}$ orbitals occupied by neutrons and protons, respectively. At low and medium spin, the alignment of protons favors prolate shape, whereas neutron alignments drive the nuclear shape towards oblate. The degree of triaxiality introduced into the system depends on the position of the Fermi surface of neutrons within the $h_{11/2}$ orbitals. Potential-energy surface calculations for nuclei in this region show minima representing prolate, triaxial, and oblate shapes becoming yrast at differ-

*Department of Physics, Indian Institute of Technology (Banaras Hindu University), Varanasi - 221005, Uttar Pradesh, India

[†]Present address : SCK-CEN, BE-2400 Mol, Belgium

[‡]Present address : IPN, F-91406 Orsay, France

[§]Present address : Dept. of Physics, University of Oslo, N-0316 Oslo, Norway

ent spins [1, 2]. Shape transition from collective prolate at lower spin to non-collective oblate shape at high spin has been observed due to alignment of valence nucleons in several nuclei of this region, see refs. [3–11].

The low- and medium-spin structure of the odd-odd Cs nuclei has been explored in detail, both experimentally and theoretically. Especially the bands with the odd proton as well as the odd neutron in $h_{11/2}$ orbitals which have been investigated. The phenomenon of signature inversion and its origin was discussed in detail, see, e.g., Refs. [12, 13]. More recently, evidence was presented for spontaneous breaking of chiral symmetry in the positive-parity bands of odd-odd $^{124-128}\text{Cs}$ [14–19]. Calculations show that the $B(M1)$ staggering in the bands, one of the characteristic features of chirality, depends strongly on the triaxiality parameter γ ; it is maximum at $\gamma = 30^\circ$ and decreases with decreasing as well as increasing γ values [20]. Recently, chirality has been investigated in ^{124}Cs [14] and it has been concluded that the nucleus remains in a chiral configuration within the spin range of $I=14-20$. At higher spin, the chiral configuration does not remain yrast due to the alignment of a pair of nucleons.

Furthermore, enhanced $B(E1)$ transition rates were measured for transitions linking positive- and negative-parity bands, indicating the existence of octupole correlations [14]. With the observation of chirality and octupole correlations, the ^{124}Cs nucleus is an example of the interplay between axially-asymmetric and reflection-asymmetric shapes. It is, therefore, interesting to investigate how nuclear shapes evolve with increasing angular momentum and what are the excitation modes prevailing in the nucleus at higher spin.

In this article, we report on an investigation of high-spin states in ^{124}Cs . All bands observed previously are extended to appreciably higher spin. Indications of band crossing have been observed in all the bands, including

chiral partner bands. The shapes of the nucleus with increasing spin and the configuration of the high-spin structures are discussed within the framework of the cranked Nilsson-Strutinsky (CNS) formalism [21–23].

In the following section, details of the experiment and the data analysis are described, followed by a presentation of the results in section III. The results are compared with CNS calculations and configurations assigned to the bands are presented in section IV. A brief summary is given in the last section.

II. EXPERIMENTAL DETAILS AND DATA ANALYSIS

High-spin states in ^{124}Cs were populated in the weak $p3n$ side channel of the $^{64}\text{Ni} + ^{64}\text{Ni}$ reaction. The ^{64}Ni beam of 265 MeV was provided by the 88-Inch cyclotron at Lawrence Berkeley National Laboratory. The Gammasphere spectrometer [24], consisting of 100 Compton-suppressed Ge detectors at the time of the experiment, were used to measure γ -ray coincidences. The target consisted of a ^{64}Ni foil of $476 \mu\text{g}/\text{cm}^2$ thickness, enriched to 96.5%. Data were recorded with a trigger condition of six or more Ge detectors after Compton suppression and 15 or more 'modules' showing a signal. A module is defined as a Ge detector and the bismuth germanate (BGO) scintillators of the suppression shields. After presorting and setting a prompt time window, a total of 1.2×10^9 events with Ge fold ≥ 4 were obtained.

The raw data were gain-matched and calibrated using standard sources. The calibrated data were then sorted into three- and four-dimensional arrays, cubes and hypercubes, respectively. The RADWARE package [25] was used for the analysis of the coincidence data. The multipolarity of the transitions was determined from two asymmetric matrices. The first one contained events detected at forward (35°) and backward angles (145°) on

were firmly established in later experiments [28, 29]. In the present work, we have extended all bands to higher spin. The observation of several inter-band transitions uniquely determines the placement of γ rays in the level scheme. Spins and parities of the known levels were adopted from previous investigations [26, 28, 29]. The partial level scheme is displayed in Fig. 1. The energy levels below spin $I = 8$ are not shown.

The positive-parity bands 1 and 2 were known up to spins 15 and 16, respectively [26]. In this work, the bands were extended up to spins 23 and 32, respectively. The intensities of these bands are smaller compared to those of the yrast positive-parity bands 3 and 4. At lower spin, the decay-out transitions linking bands 2 and 3 are stronger than the in-band transitions. Therefore, new transitions of bands 1 and 2 are best visible in gated spectra involving decay-out transitions, see Figs. 2 (a) and (b), respectively. The presence of a second 1000-keV transition in band 2 is validated in Fig. 2 (c) where triple gates involving the 644- and 1000-keV transitions of the band show a peak at 1000 keV. A branch consisting of the 916- and 1244-keV γ rays has been observed in parallel to the 936- and 1224-keV transitions of band 2. This is displayed in Figs. 2 (d) and (e), where the first branch is missing in the gated spectrum involving the 1224-keV γ ray and the second one is missing involving the 1244-keV gate. Furthermore, four new transitions linking bands 2 and 3 have been observed, see Figs. 3 (a)-(d). The intensity of the decay-out transitions decreases drastically with increasing spin and, hence, they are observed only in summed spectra with selected gating transitions. The intensity ratio, R_θ , for the transitions of band 2 are consistent with their stretched quadrupole character (see Table I). Two branches, A and B, see Fig. 1, have been observed to feed the $I^\pi=12^+$ and 14^+ states of band 2. The R_θ values measured for some of these transitions are compatible with their dipole character.

Band 3 was known up to spin and parity $I^\pi = 21^+$ [26], which was extended by Komatsubara *et al.* [27] by placing three more transitions on top of the band. However, spins were not assigned to the new levels in the later work. In this experiment, the band has been extended to a tentative spin of $I = 37$. In addition, a couple of side branches, feeding the band at higher spin, and a few inter-band transitions between bands 3 and 4 have been observed. A summed triple-gated spectrum, displayed in Fig. 4 (a), shows the new transitions of band 3. The multipolarities determined for some of the new transitions are consistent with their stretched $E2$ character. For transitions from higher-spin states, $E2$ multipolarity has been assumed as they belong to a collective rotational cascade.

Band 4 was established up to spin $I^\pi = 22^+$ in the work by Gizon *et al.* [26] and was assigned as signature partner of band 3. Two transitions with energies of 1270 and 1255 keV were added to the band by Komatsubara *et al.* [27]. In the present work, it has been established that these γ rays are not in coincidence with each other. Therefore, the 1255-keV transition has been placed in a side branch of band 4 (see Fig. 1). The band has been further extended to spin and parity $I^\pi = 30^+$. The new transitions are visible in the triple-gated spectrum displayed in Fig. 4 (b).

Negative parity was assigned to bands 5 and 6, and they were interpreted as signature partner bands [26]. Several decay-out transitions from these bands to the positive-parity bands 3 and 4, were reported previously [14, 28, 29]. These transitions are also observed in the present experiment. A new decay-out transition has been placed between the 19^- state of band 5 and the 18^+ level of band 4. Furthermore, band 5 has been extended to spin and parity $I^\pi = (31^-)$. Two side branches, 5A and 5B, have been observed to feed band 5 at spins 25 and 29, respectively. With the help of the multipolarity mea-

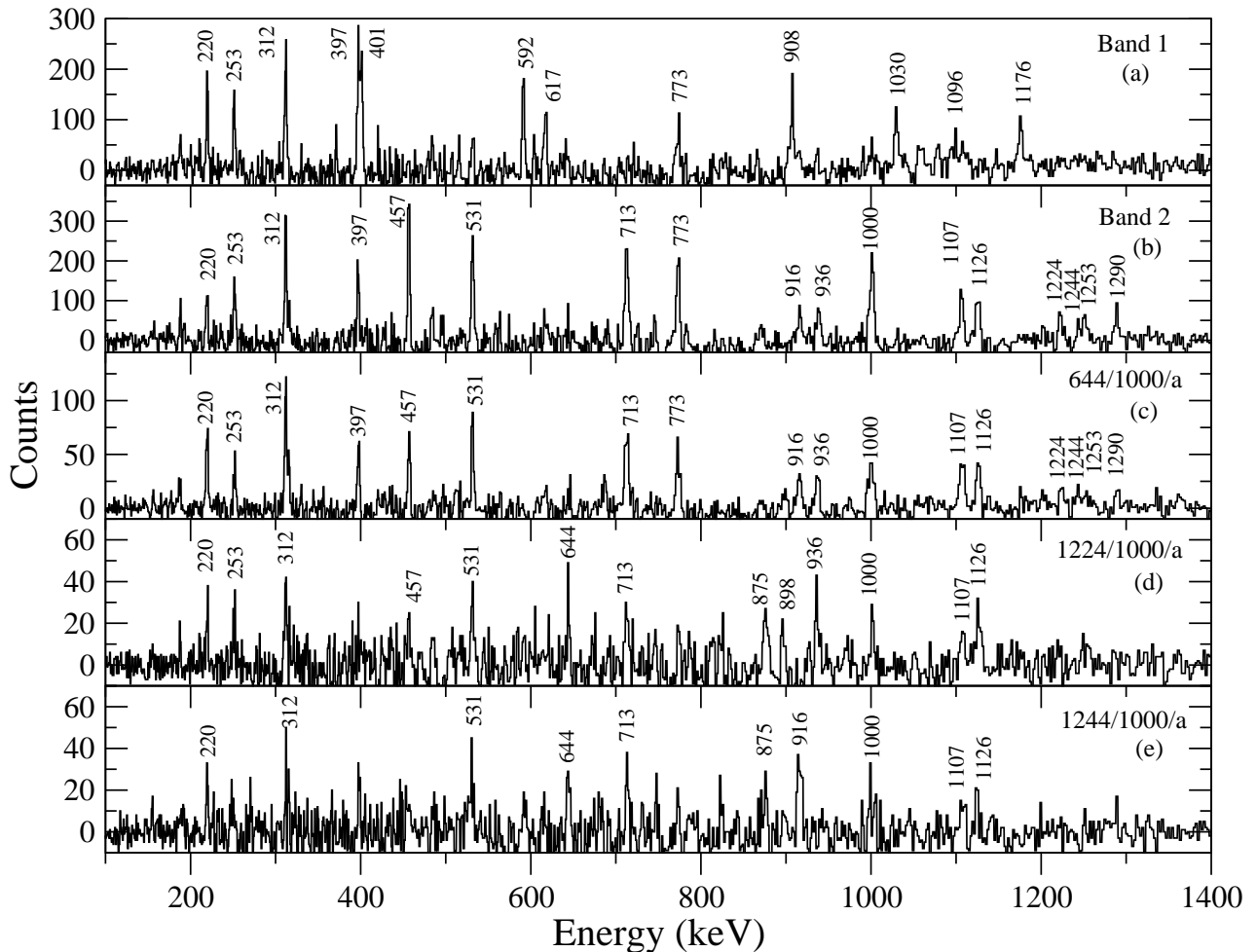


FIG. 2: Summed triple-gated spectra showing γ rays of (a) band 1, (b) band 2. For band 1 gates were set on the 312-, 617-, 592-, 401-, 908-, 1030-, and 1176-keV γ rays, whereas for band 2 two gates were taken from a list of all the transitions above the 16^+ level and the third gate was set on the 644-keV decay-out transition. The presence of a second 1000-keV transition in band 2 is displayed in panel (c) where triple gates were set on 644 keV, 1000 keV, and a transition from a list “a” consisting of the 220-, 312-, 316-, 397-, and 457-keV transitions of bands 3 and 4. The parallel branches consisting of (916 and 1244) and (936 and 1224) of band 2 are shown in panels (d) and (e). The spectra are created with a first gate on 1224 keV (d) and 1244 keV (e); the second gate on the 1000-keV γ ray and the third gate is one of the transitions from the list “a”.

sured for the connecting transitions, spins and parities have been assigned to the lowest levels of the branches. Similarly, band 6 has been extended to $I^\pi = (34^-)$. Several new transitions, most likely of $M1$ character, have been placed linking bands 5 and 6. The new transitions of bands 5 and 6 can be observed in Figs. 4 (c) and (d), respectively.

Four new transitions (see Fig. 4 (e)) have been added to band 7 above the previously known state at $I^\pi = (23^-)$ [27]. Thus, the band has been extended to the level with spin $I = (31^-)$. Decay-out transitions of 334 and 415 keV were observed between bands 7 and 6. A new 457-keV transition has been added to these decays. Furthermore, band 7 also decays to band 4 through the 868- and 987-keV transitions.

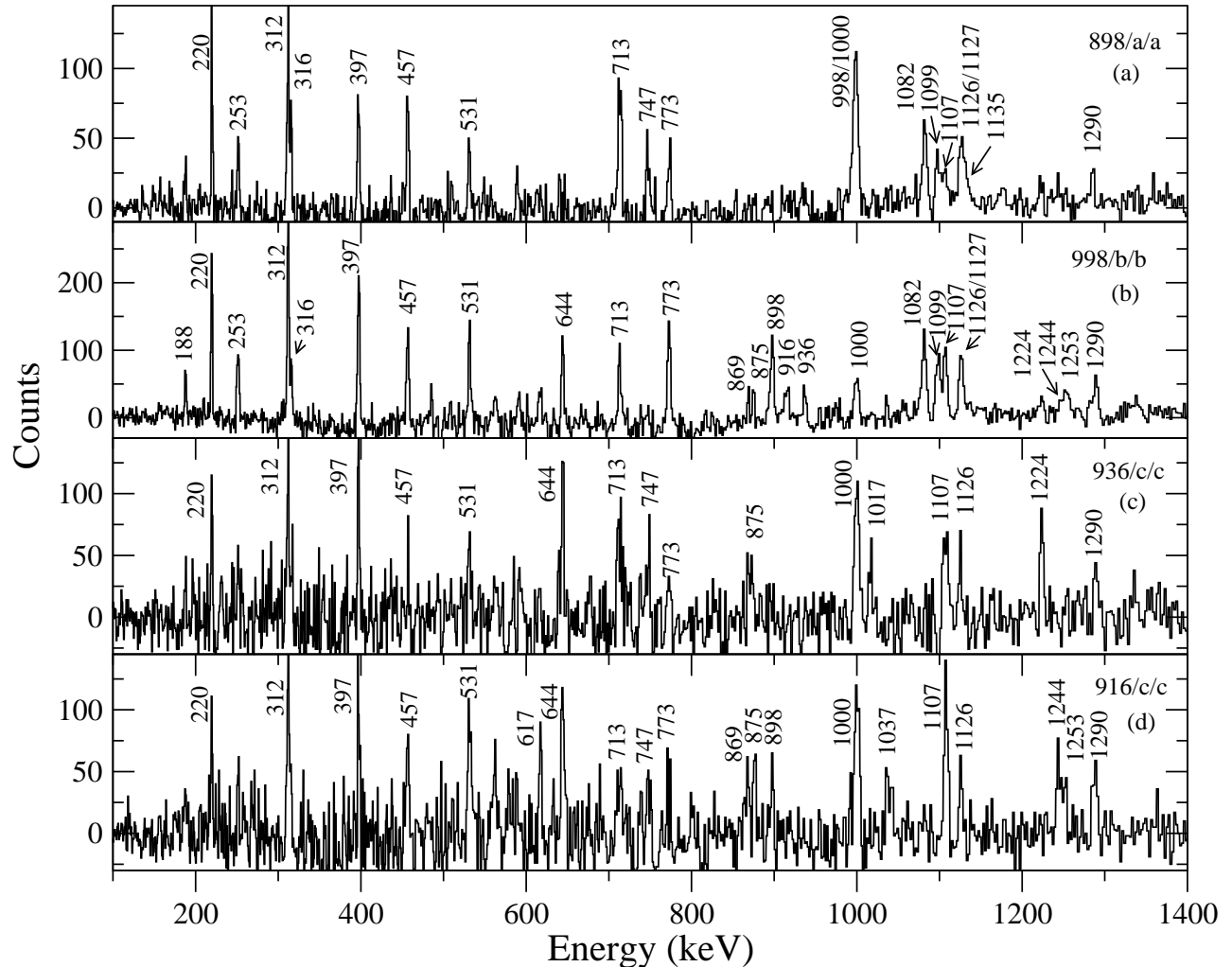


FIG. 3: The decay-out transitions (a) 747 keV, (b) 875 keV, (c) 1037 keV, and (d) 1017 keV from band 2 are seen in triple-gated spectra. The gates used to generate these spectra are shown at the top right corner of each panel. The list “a” includes the 220-, 312-, 316-, 397-, and 457-keV transitions of bands 3 and 4, “b” includes the 312-, 220-, 397-, 773-, and 898-keV γ rays and “c” consists of all the transitions of list “a” and the 485-, 773-, 898-, and 998-keV γ rays.

Three transitions of band 8 were observed by Gizon *et al.* [26]. However, the band was not reported in later investigations [27–29]. In this work, six new transitions have been observed in coincidence with the known low-energy transitions of the band and are shown in Fig. 4 (f). The band is populated with the lowest intensity among the bands of ^{124}Cs . The low intensity of the transitions does not allow to determine their multipolarities. The tentative spin and parity assignments to the band

were adopted from previous work [26]. Assuming their $E2$ character, the band is tentatively extended to spin $I^\pi = (26^-)$. Two decay-out transitions of 532 and 753 keV have been observed from band 8 to band 6.

IV. DISCUSSION

In this section, the configurations of the bands are discussed. Arguments for the configuration assignments

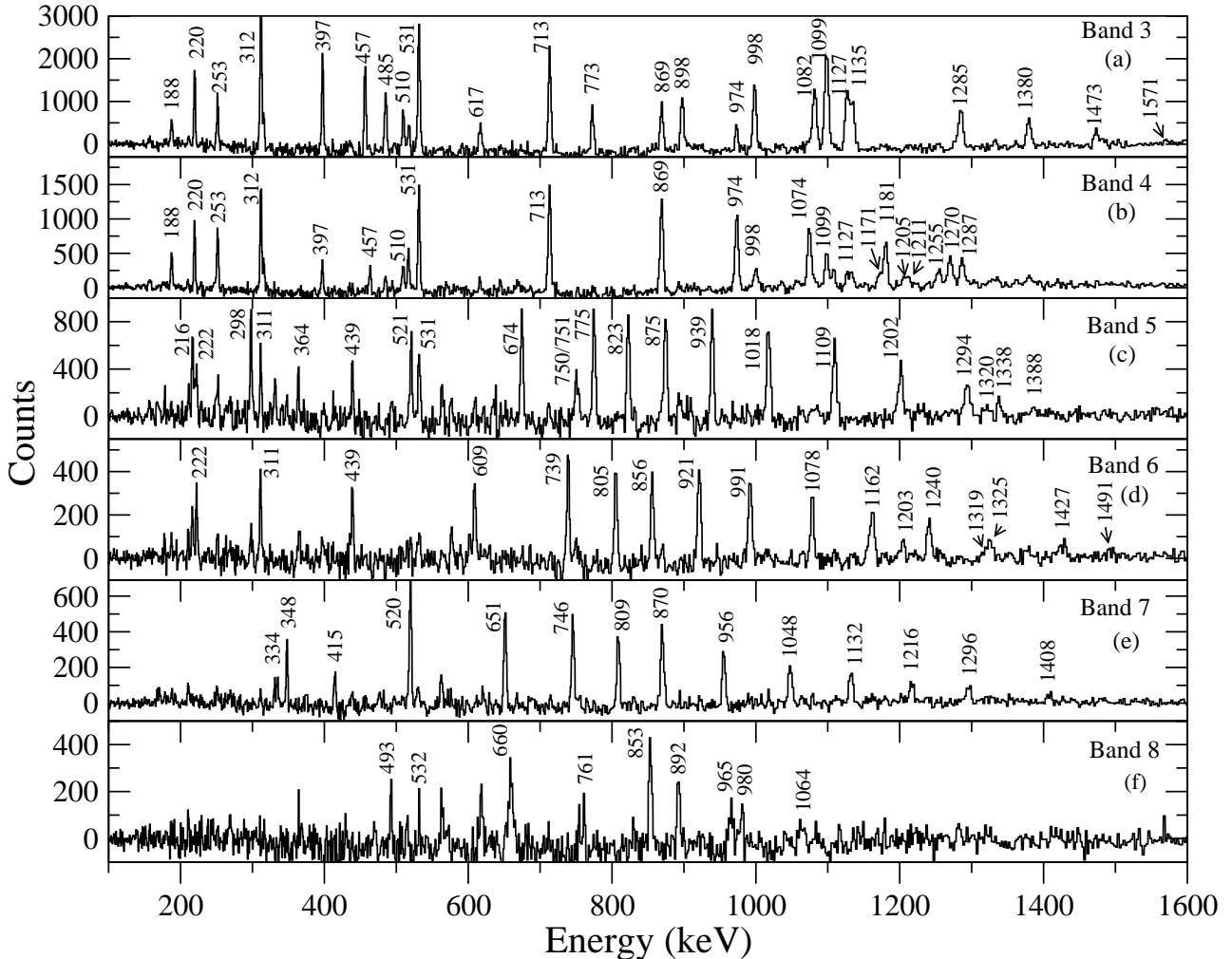


FIG. 4: Summed triple-gated spectra for bands 3-8 of ^{124}Cs . The gates were set on all the transitions of each band.

are the observed excitation energies, band-crossing frequencies, and alignment gains. These quantities can be compared with those observed in the neighboring nuclei as well as with the results of theoretical calculations. For the medium- and high-spin states, calculations have been performed using the configuration-dependent cranked Nilsson-Strutinsky (CNS) formalism [21–23].

In the CNS formalism, the orbitals in each \mathcal{N} -shell are grouped into high- j and low- j shells, respectively. Each group of orbitals can be further divided according to signature, $\alpha = 1/2$ and $\alpha = -1/2$. The configurations are

then labeled by the number of particles or holes in each group. No separation into core and valence particles is made and all the orbitals up to $\mathcal{N} = 8$ are treated on an equal footing. It is only necessary to define the filling of the valence shells, because the low- \mathcal{N} shells are fully occupied while the orbitals in the high- \mathcal{N} shells are empty in the low-energy configurations of ^{124}Cs . The configurations in this model are labeled as

$$[p_1 p_2, n_1 n_2].$$

Here, p_1 and p_2 are the number of protons in $g_{7/2}d_{5/2}$

and $h_{11/2}$ orbitals, respectively, whereas n_1 and n_2 are the number of neutron holes in gds orbitals and neutron particles in $h_{11/2}$ orbitals, respectively. Note that in most of the previous publications, e.g. Ref. [30], configurations have been labeled only by the number of high- j particles, i.e. $[p_2, n_2]$. Here, longer labels are used, mainly because, when appropriate, the signature within the different groups can be specified by a subscript, + for $\alpha = 1/2$ and $-$ for $\alpha = -1/2$.

In the present calculations, for the κ and μ parameters defining the $l \cdot s$ and l^2 strengths of the modified oscillator potential, the so called A ~ 110 parameters have been used [30]. Excitation energies are calculated from the sum of the shell energy and the rotating liquid-drop energy. The latter is modeled according to the Lublin-Strasbourg drop model [31] with the rigid body moments of inertia calculated with a radius parameter of $r_0 = 1.16$ fm and a diffuseness parameter of $a = 0.6$ fm [23]. The energy of each configuration is minimized at each spin in the deformation space $(\varepsilon_2, \varepsilon_4, \gamma)$, which makes it possible to follow the development of collectivity in each individual configuration as a function of spin. Pairing is not included in the model, which implies that the calculated results are relevant at higher spins, where pairing is quenched. However, the agreement is also satisfactory at intermediate spins ($I > 15$ in the mass-125 region); see, e.g., Refs. [3, 6–10].

The low-energy non-collective (not shown in Fig. 1) and collective level structures of ^{124}Cs were explained previously in terms of single-particle excitations within the Interacting Boson-Fermion-Fermion Model (IBFFM) [26]. For the collective bands, the configurations were also explored using the Woods-Saxon cranked Shell Model (CSM) [26]. In the following, the configurations of the positive- and negative-parity bands are discussed within the framework of the CNS formalism.

A. Positive-parity bands: Bands 1-4

Bands 3 and 4 are the yrast sequences among the positive-parity states and are signature partners. The configuration $\pi h_{11/2} \otimes \nu h_{11/2}$ was suggested previously for these bands [26, 29]. Band crossings, indicative of configuration change, were observed at rotational frequencies 0.55 MeV and 0.63 MeV in the $\alpha=1$ and $\alpha=0$ signatures, respectively [26]. Alignment of a pair of $h_{11/2}$ neutrons was suggested for these crossings [26]. The above configuration has also been assigned to bands 1 and 2 [26, 29]. In a recent work, it has been suggested that the low-energy states of bands 1-4 are due to spontaneous breaking of chiral symmetry [14]. In the present work, these bands are extended to higher spin and band crossings have been observed for the first time in bands 1 and 2. In the following, configurations of the bands are discussed within the framework of the CNS model and a detailed analysis of the crossings and the alignment gain is presented.

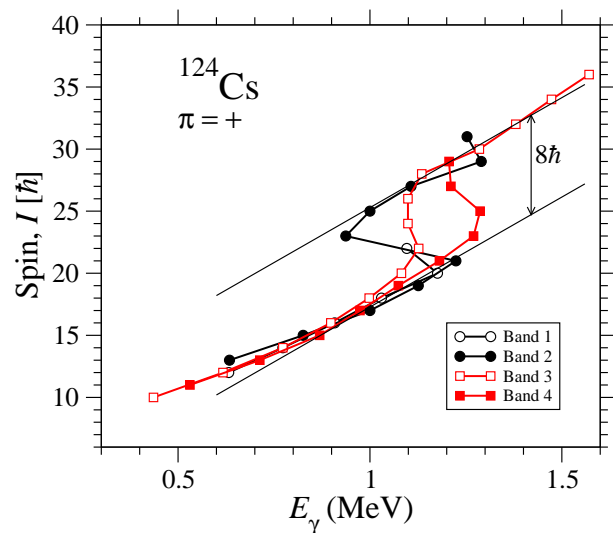


FIG. 5: (Color online) Spin versus transition energy for the observed positive-parity bands in ^{124}Cs . Two parallel lines are drawn with a spin difference of $8\hbar$ to highlight the alignment gain at the band crossing. In this and other figures, even-spin states ($\alpha=0$) are drawn by filled symbols and odd-spin states ($\alpha=1$) by open symbols.

The spins of bands 1 – 4 are plotted as a function of

transition energy in Fig. 5. The slope of the curves represents the kinematic moments of inertia, $\mathcal{J}^{(1)}$, of the bands. Both pairs of bands, bands 1-2 and 3-4, have similar moments of inertia at lower spin. The slopes continue to be similar for the extended portion of bands 2 and 3 beyond the alignment of nucleons. This indicates that the underlying configurations of both pairs of bands are also similar at higher spin. With the extension of bands 1 and 2 to higher spin, band crossings around $\hbar\omega \simeq 0.52$ MeV are observed in both bands with an alignment gain of $8\hbar$, see Fig. 5. This indicates that the nature of the aligning particles is the same in both pairs of bands. A small difference in alignment frequency may be due to different deformation of the bands.

Potential-energy surfaces calculated as a function of angular momentum for the positive-parity and signature $\alpha = 0$ states are shown in Fig. 6. There are essentially four minima in these surfaces. Typical configurations at the respective minima are illustrated in Fig. 7. Consider first the minimum labeled I, which is located at oblate collective shape ($\gamma = -60^\circ$) at low spin. With increasing spin it moves towards $\gamma = -40^\circ$ and disappears at $I \approx 30$. This minimum is built from the [41,65] configuration which is calculated in the yrast region from low spin up to $I \approx 25$. There are two minima at close to prolate shape at low spin, one labeled II at $\varepsilon \approx 0.22$ and another one labeled III at $\varepsilon \approx 0.30$. The former minimum is built from the [50,76] configuration at low spin. The corresponding band moves away from yrast at $I \approx 20$, where the [41,65] configuration takes over. The energy surfaces in Fig. 6 are drawn for signature $\alpha = 0$ while, as seen in Fig. 7, the $\alpha = 1$ band comes much lower in energy in the spin range $I = 20$ up to termination around $I = 40$. The second prolate minimum at $\varepsilon \approx 0.30$ is formed with two $g_{9/2}$ proton holes in the $Z = 50$ core, i.e., a [(02)61,87] configuration where '02' in parentheses is the number of $\mathcal{N}=3$ and $g_{9/2}$ holes, respectively.

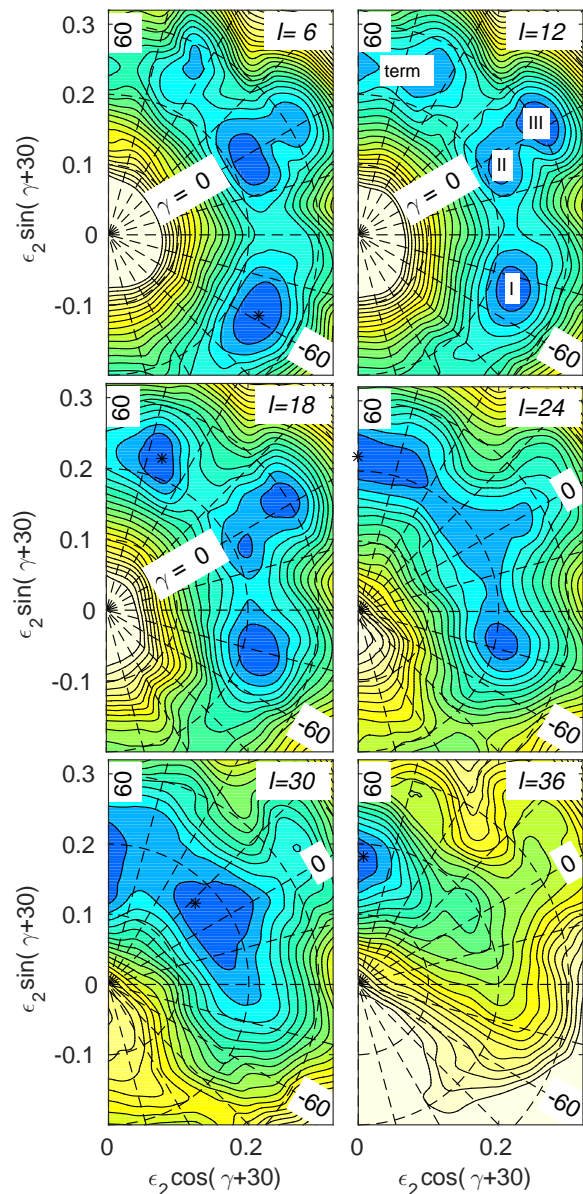


FIG. 6: (Color online) Potential-energy surfaces with the constraint, $\pi = +$, $\alpha = 0$. The labeling of the different minima is illustrated in the $I = 12$ surface. The contour-line separation is 0.25 MeV.

However, this configuration moves away from yrast for spin values above $I = 20$. The fourth minimum labeled 'term' is formed at γ -values of $40^\circ - 60^\circ$, mainly corresponding to configurations which come down into the yrast region and terminate at specific spin values. Such terminations forming yrast states are seen for many spin values but those formed as the maximum spin states in specific configurations are most interesting; especially the

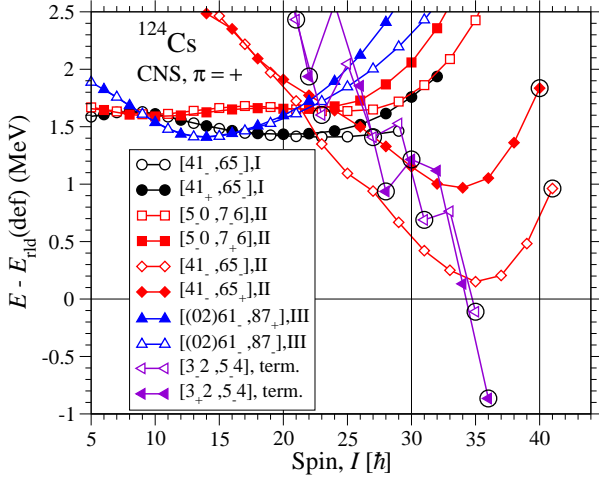


FIG. 7: (Color online) The energy of low-lying positive-parity configurations in the different minima of Fig. 6 are shown relative to the rotating liquid drop energy. As illustrated in Fig. 6, the minimum around $\gamma = -40^\circ$ is labeled as I, the two close-to-prolate minima at $\varepsilon_2 \approx 0.22$ and $\varepsilon_2 \approx 0.30$ as II and III, respectively. The minima at or close to $\gamma = 60^\circ$ are labeled as “term”, indicating that most of these configurations terminate in non-collective oblate states.

[32,54] configuration which terminates at $I = 36$ in the configuration

$$\pi(d_{5/2}g_{7/2})^3_{8.5}(h_{11/2})^2_{10}\nu(d_{3/2})^1_{1.5}(h_{11/2})^4_{16}.$$

Considering the very favored energy of this state (see Fig. 7), the prediction that it is yrast appears very reliable and it would be interesting to look for it in future experiments.

There are interesting similarities between the predicted terminations in the present mass region with approximately 10 particles outside the ^{114}Sn core and the well established terminations in nuclei around ^{158}Er with 10-12 particles outside the ^{146}Gd core, see Refs. [3, 4, 33].

The energy surface calculations might be compared with previous calculations of the nuclear shape of the positive-parity bands in ^{124}Cs . Total routhian surfaces were calculated in Ref. [26], where prolate shape at $\beta_2 \approx 0.24$ and $\beta_2 \approx 0.18$ was predicted before and after the alignment region, respectively. This is consistent with the low-lying minimum II calculated at $\varepsilon \approx 0.22$ (see above), which moves towards decreasing quadrupole de-

formation with increasing spin. One should note, however, that according to our calculations, this minimum is formed from the [50,76] configuration at low spin and not from the [41,65] configuration. The self-consistent triaxial relativistic mean field approach was applied to the $\pi(h_{11/2})^1\nu(h_{11/2})^1$ configuration in Ref. [34]. In agreement with our calculations, triaxial shape is obtained but with rather different values of the γ -parameter, $\gamma = 22^\circ$ compared with our predictions of γ -values in the $-60^\circ - -40^\circ$ range. Because the relativistic calculations are carried out at static shape, the sign of γ is irrelevant but even so, the triaxiality appears to be rather different in the two calculations.

Three different configurations are calculated in the yrast region which lie at a similar energy in the $I \leq 20$ spin range, see Fig. 7. However, the two configurations at close to prolate shape move away from yrast for $I > 20$ while the observed bands 3 and 4 lie low in energy up to or above $I = 30$. Furthermore, the negative- γ configuration $\pi(h_{11/2})^1\nu(h_{11/2})^5$ appears higher in energy when approaching $I = 30$. However, it shows up low in energy at close to prolate shape. It turns out that this jump in deformation provides a good description of the observed backbends in the positive-parity bands. Thus, from the CNS calculations, the same conclusion is drawn as in the previous studies, see, e.g., Refs. [14, 26, 27], namely that the positive-parity yrast bands 3 and 4 are formed in the $\pi(h_{11/2})^1\nu(h_{11/2})^5$ configuration. Note that while all particles in a j -shell or groups of j -shells are specified in the present CNS formalism, only those particles which are considered as aligned are specified in several other formalisms.

According to the discussion above, bands 3 and 4 should be assigned to the [41,65] configuration with a triaxial close to oblate shape at low spin and a transition to close to prolate shape at the band crossing just above $I = 20$. It seems natural to assign the same configuration also to

the partner bands 1 and 2 because four bands are formed from the combination of $\alpha = \pm 1/2$ signature for protons and neutrons. This assignment is in agreement with the predicted chiral symmetry in the $I = 10 - 20$ spin range of these bands even though the calculated deformation is rather far from the optimal value, $\gamma = 30^\circ$ (or -30°).

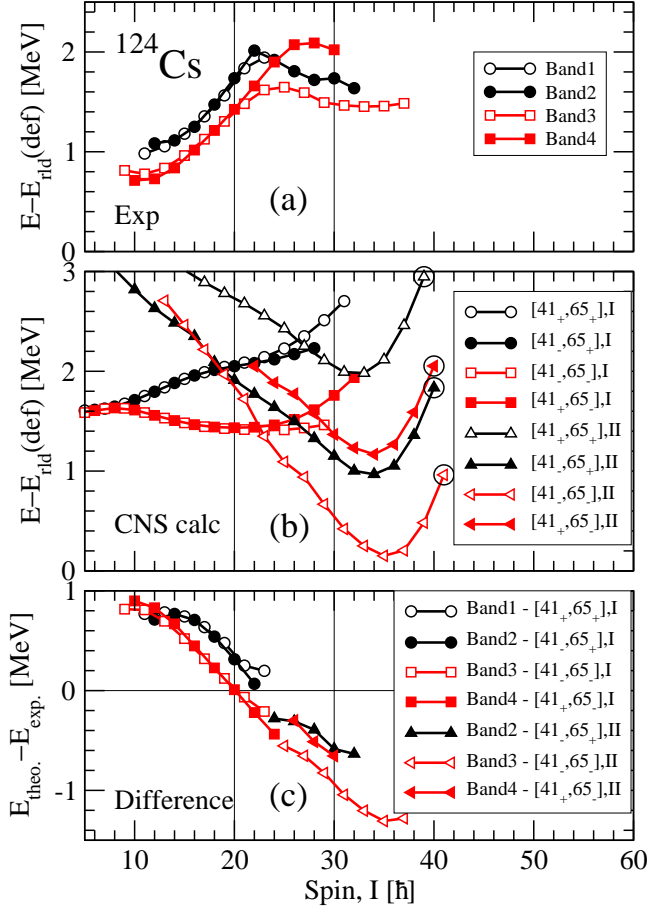


FIG. 8: (Color online) (a) Experimental excitation energies relative to the rotating liquid drop energy of the positive-parity bands of ^{124}Cs . (b) Calculated excitation energies relative to the same reference for the $[41,65]$ configuration. Values calculated at minimum I (see caption to Fig. 7) are drawn by circles and squares and those at minimum II by triangles. (c) Difference between the experimental and calculated excitation energies. Experimental values before the band crossings are compared with values from minimum I and those after the band-crossing with values from minimum II.

The observed bands 1-4 are compared with the bands resulting from the $[41,65]$ configuration calculated in the CNS formalism in Fig. 8. The fact that all differences between theory and experiment are calculated within ± 0.2 MeV with a smooth slope proves that the relative ener-

gies are well reproduced in the CNS calculations; especially the fact that the curves continue smoothly through the crossing region at $I = 20 - 25$ indicates that the calculated shape change gives rise to an alignment roughly in agreement with experiment. Furthermore, the smooth down-slope of the difference curves in Fig. 8 is what would be expected when pairing is not included, see Refs. [35, 36]. In Fig. 8, one notes that, at low spin, the calculations predict that the two signatures of the $h_{11/2}$ proton are degenerate. This is expected at the bottom of a high- j shell at oblate or close to oblate shape. After the band-crossing a splitting is observed. Here, the two lowest calculated bands differ by the signature of the $h_{11/2}$ neutron and at prolate shape, the proton orbital at the bottom of the high- j shell has a large signature splitting. These predictions are consistent with experiment. While band 4 is the lowest $\alpha = 0$ band at low spin, it is crossed by band 2 which becomes the lowest $\alpha = 0$ band after the band crossing; giving further support to the predicted shape change.

It is also interesting to note that band 3 appears to be only two transitions short of smooth termination [30] in a maximum spin state. Thus, the $[41-, 65-]$ configuration which is assigned to band 3 terminates at $I = 41$ in the configuration

$$\pi(d_{5/2}g_{7/2})_{10}^4(h_{11/2})_{5.5}^1\nu(d_{5/2}g_{7/2})_6^{-2}(d_{3/2}s_{1/2})_2^2(h_{11/2})_{17.5}^5,$$

where the maximum spin in the different groups is shown by a subscript. It should be possible to observe this terminating state which is calculated around 1 MeV above yrast. The experimental trends, according to the upper panel of Fig. 8, rather suggest that it will come closer to yrast.

The band crossings in the positive-parity bands in ^{124}Cs , and similar band crossings in ^{123}Cs and ^{123}Xe , have previously been assigned as paired crossings based on $h_{11/2}$ neutrons [3, 26, 32]. However, with the full band crossing

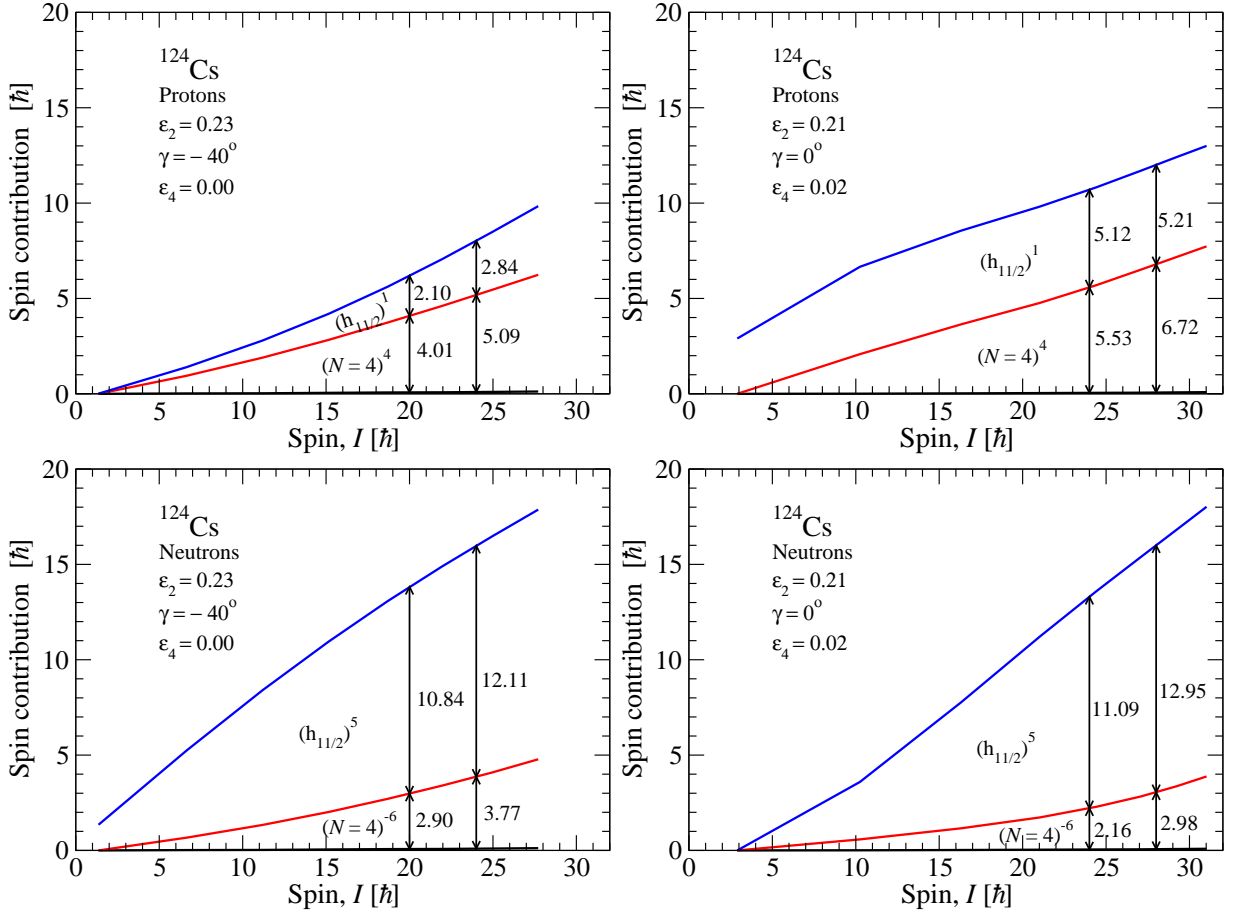


FIG. 9: (Color online) Spin contribution in the $[41-, 65-]$ configuration of ^{124}Cs at the approximate deformations calculated for $I = 24$, $\varepsilon_2 = 0.23$, $\gamma = -40^\circ$, $\varepsilon_4 = 0.00$ (minimum I) and $\varepsilon_2 = 0.21$, $\gamma = 0^\circ$, $\varepsilon_4 = 0.02$ (minimum II), respectively. It is illustrated how the total spin is built with a tiny contribution from the core (the $\mathcal{N}=0-3$ shells for either protons or neutrons) and then successively from the alignment of particles in different j - or \mathcal{N} -shells. The contribution from the six $\mathcal{N}=4$ neutron holes is calculated as the sum of spin contributions from the 24 filled $\mathcal{N}=4$ orbitals. The spin contribution at spin values 20, 24 and 24, 28, respectively is specified. For example, for protons at $I = 24$ in the prolate minimum, the four $\mathcal{N}=4$ protons contribute with $5.53\hbar$ and the $h_{11/2}$ proton with $5.12\hbar$, while the contribution from the core is smaller than $0.1\hbar$.

identified in ^{124}Cs , the alignment gain in the positive-parity bands is around $8\hbar$, see Fig. 5. This value is too large for an alignment based on an odd number of particles in the middle of an $h_{11/2}$ shell. The present calculations do instead suggest that the crossing is mainly caused by a deformation change as discussed above. Indeed, the crossing is well described in the CNS formalism without pairing even though the alignment gain is somewhat underestimated. This suggests that pairing only plays a minor role in the observed band crossings.

Within the CNS formalism, it is straightforward to determine how the spin is built in different configurations.

In order to illustrate this, we choose deformations close to those calculated for the $[41-, 65-]$ configuration in the crossing region around $I = 24$ in the minima at $\gamma \approx -40^\circ$ (minimum I) and $\gamma \approx 0^\circ$ (minimum II). At these deformations, the spin contribution from the different j -shells or \mathcal{N} -shells is illustrated in Fig. 9. When comparing the two deformations in this figure, the most striking difference is that the protons are much easier to align at prolate deformation than at $\gamma = -40^\circ$. For example, at $I = 24$, the protons contribute with only around $8\hbar$ at the triaxial deformation but with almost $11\hbar$ at prolate deformation. This is in agreement with general rules

that few particles in high- j shells are easy to align at prolate shape in contrast to oblate or close-to-oblate deformations, see e.g. Refs. [37, 38] or diagrams of how particles align in high- j shells, see e.g. Ref. [39]. The $h_{11/2}$ neutrons are more difficult to align at $\gamma = 0^\circ$ than at $\gamma = -40^\circ$, e.g. at $I = 24$, they contribute with $11.1\hbar$ at the former deformation but with $12.1\hbar$ at the latter.

At the band crossing, the spin jumps from $I \approx 20$ to $I \approx 28$ at a fixed frequency, see Fig. 5. It is instructive to investigate how the spin is built at $I = 20$ in minimum I and $I = 28$ in minimum II, see Fig. 9. The spin increase from the $I = 20$ state in minimum I to the $I = 28$ state in minimum II is built by $2.7\hbar$ from the four $\mathcal{N}=4$ protons, by $3.1\hbar$ from the single $h_{11/2}$ proton, and by $2.1\hbar$ from the five $h_{11/2}$ neutrons, while the contributions from the $\mathcal{N}=4$ neutron holes and the core are very small. Thus, according to the CNS calculations, the spin increase at the band crossing gets its largest contribution from the alignment of the protons in the close-to-prolate minimum. Pairing could give corrections to this picture but the fact that the different bands and their crossings are so well described without pairing indicates that such corrections will be rather small. Consequently, previous descriptions [26, 27] of the crossing as $\nu(h_{11/2})$ appear incorrect.

B. Negative-parity bands: Bands 5-8

The negative-parity bands 5 and 6 are signature partners and the configuration $\pi h_{11/2} \otimes \nu(g_{7/2}d_{5/2})$, was suggested for the bands [26]. The measured $B(M1)/B(E2)$ ratios were consistent with the values calculated using the geometrical model of Dönau and Frauendorf [40, 41] for the above configuration [26]. Band crossings have been observed in both bands at a frequency of $\hbar\omega \sim 0.42$ MeV, very close to the values $\hbar\omega \sim 0.44$ and 0.41 MeV observed for the band crossings in the favored and unfavored bands

in the neighboring ^{123}Cs nucleus. The band crossings in ^{123}Cs have been interpreted as caused by the alignment of a pair of $h_{11/2}$ neutrons [3]. An alignment gain of nearly $5\hbar$ (see Fig. 10) is also in agreement with the value obtained from cranking calculations [26]. Thus, the most likely configuration of the aligned particles in the bands above the crossing is $\pi h_{11/2} \otimes \nu[(h_{11/2})^2(g_{7/2}d_{5/2})]$.

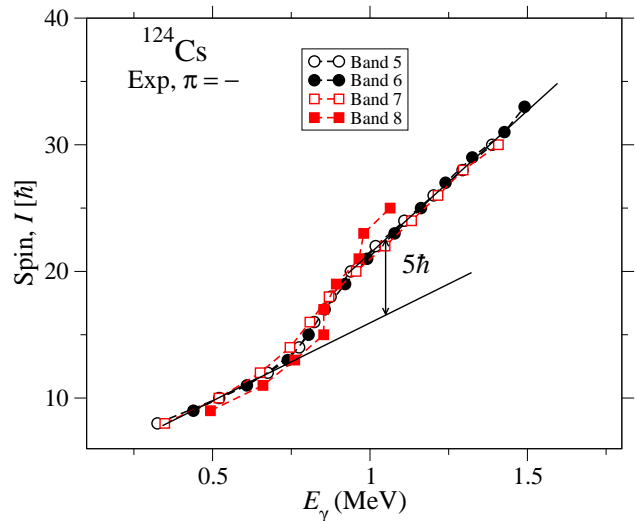


FIG. 10: (Color online) Spin versus transition energy for the observed negative-parity bands in ^{124}Cs . The alignment gain of $5\hbar$ at the band crossing has been shown through two straight lines.

Band 7 was tentatively assigned the $\pi h_{11/2} \otimes \nu(g_{7/2}d_{5/2})^1$ and $\pi h_{11/2} \otimes \nu[h_{11/2}^2(g_{7/2}d_{5/2})^1]$ configurations before and after the band crossing, respectively, i.e., the same as that of bands 5 and 6. A possibility that band 8 could be its signature partner was also discussed [26]. Both, bands 7 and 8, show a crossing at $\hbar\omega \sim 0.42$ MeV with an alignment gain of nearly $5\hbar$ (see Fig. 10), and band 8 shows an additional alignment of $\sim 2\hbar$ below $\hbar\omega = 0.5$ MeV indicating some special property of this band, e.g. a shape change.

Calculations using the CNS model have been performed to search for probable configurations of the bands. Potential-energy surfaces for even spin and negative parity are displayed in Fig. 11. The different minima and their evolution with spin are similar to the positive-parity

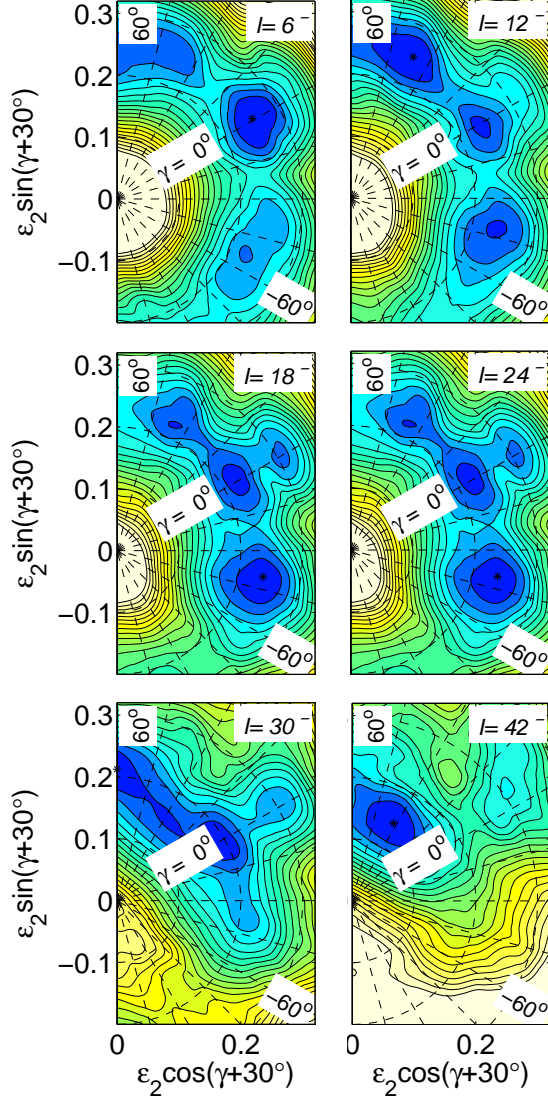


FIG. 11: (Color online) Potential-energy surfaces with the constraint, $\pi = -$, $\alpha = 0$. The contour line separation is 0.25 MeV.

surfaces in Fig. 6. For negative parity, there is a competition between the $[41,76]$ and $[50,65]$ configurations. The corresponding bands in the different minima are drawn relative to the rotating liquid-drop reference in Figs. 12 and 13. At low spin, up to $I \approx 10$, another configuration with one $g_{9/2}$ proton hole and with seven $h_{11/2}$ neutron particles is low in energy at prolate shape. In the $I^\pi = 6^-$ energy surface, the prolate minimum corresponding to this configuration is clearly lowest. At higher spin values, there are several minima at similar energies

as for positive parity (see above). The minimum labeled I at $\gamma \simeq -40^\circ$ disappears around $I = 30$ while the prolate minimum labeled II at $\varepsilon_2 \approx 0.20$ for low spin moves towards termination at higher spin values, as is clearly seen in the $I = 30$ and $I = 42$ energy surfaces. Furthermore, the prolate minimum labeled III at $\varepsilon_2 \approx 0.30$, which is built with two $g_{9/2}$ proton holes, appears at intermediate spin values in a similar way as for positive parity and also the positive-gamma minimum at $\gamma = 35^\circ - 60^\circ$ shows up in a similar way as for positive parity.

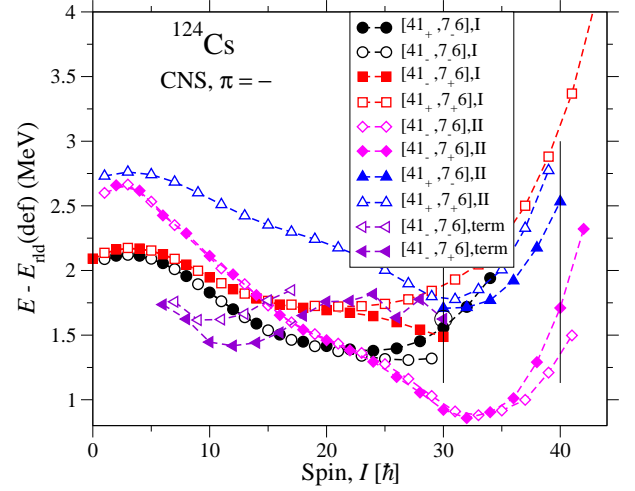


FIG. 12: (Color online) Calculated bands in the $[41,76]$ configuration at three different shapes, triaxial at $\gamma \approx -40^\circ$ (I), near-prolate (II), and triaxial at $\gamma \gtrsim 30^\circ$ (term) where the labeling of the minima is illustrated in Fig. 6 and explained in the caption of Fig. 7.

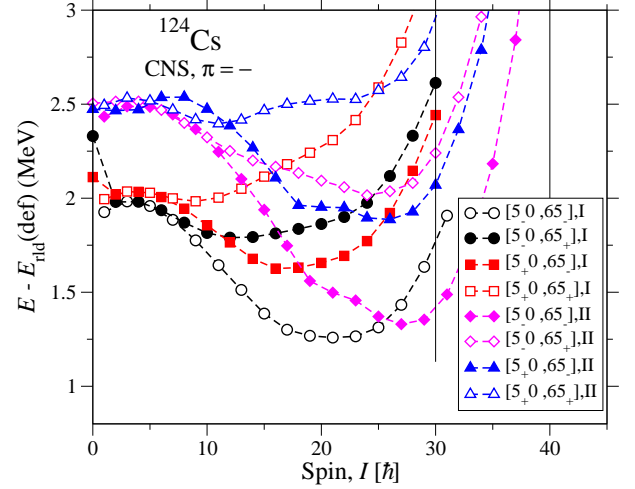


FIG. 13: (Color online) As Fig. 12 but for the $[50,65]$ configuration.

In order to find an interpretation for the observed bands, configurations which form extended collective bands in the yrast region should be considered. The only possibilities seem to be the [50,65] or the [41,76] configurations. Relative to the favored positive-parity configurations [41,65], they are formed with either one less $h_{11/2}$ proton or one additional $h_{11/2}$ neutron. As seen in Figs. 12 and 13, these configurations form bands at $\gamma \approx -40^\circ$ and $\gamma \approx 0^\circ$ at similar energies in the $I \simeq 20$ spin range, but the prolate [41,76] configuration comes clearly lowest in energy when approaching $I = 30$.

In experiment, three bands show a similar evolution with spin up to $I \approx 30$. As the different calculated bands are very scattered for the [50,65] configuration, this suggests that the observed bands are rather built from the [41,76] configuration where pairs of signature degenerate bands are calculated in extended spin ranges. Therefore, it can be assumed that the observed bands are mainly built from the $\pi(h_{11/2})^1\nu(h_{11/2})^6$ configuration in agreement with previous assignments [26].

Bands 5 and 6 are signature degenerate at low spin and stay close together also at high spin, see upper panel of Fig. 14. Comparing with Fig. 12, they are naturally assigned to the prolate $[41_-, 7_\pm 6]$ configuration at high spin, $I = 20 - 30$. These bands show an alignment of $\sim 5\hbar$ around $I = 15$, see Fig. 10. This alignment may be explained by the calculated crossing between prolate and $\gamma \approx -40^\circ$ [41,76] configurations. A closer look reveals, however, that the $h_{11/2}$ proton leads to the signature degeneracy at $\gamma \approx -40^\circ$, while it gives rise to a large signature splitting at prolate shape and the signature degeneracy is caused by the $\mathcal{N}=4$ neutrons. Thus, for the even-spin states, the low-spin band $[41_+, 7_- 6]$ crosses the $[41_-, 7_+ 6]$ band. For the positive-parity bands, the shape change from $\gamma \approx -40^\circ$ to $\gamma \approx 0^\circ$ was supported by a similar comparison of the favored signatures before and after the band crossing.

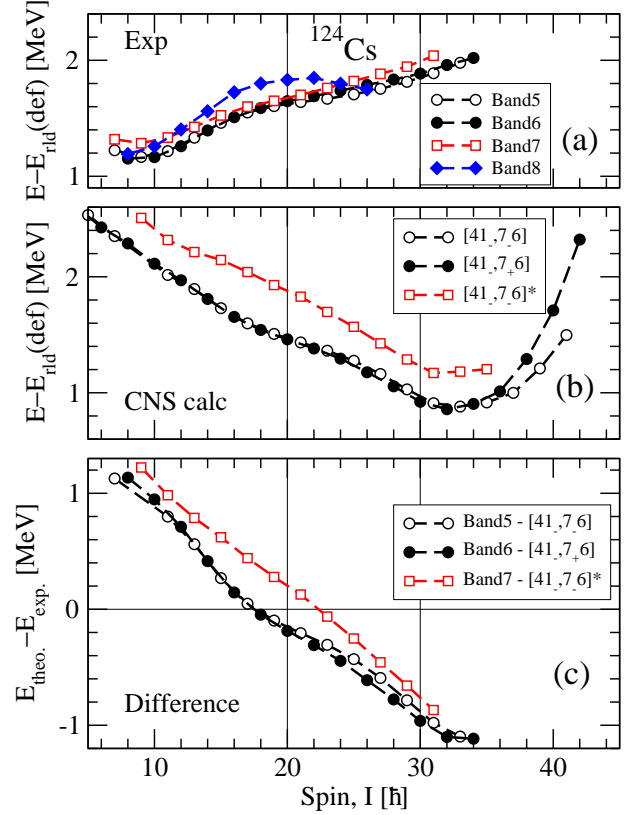


FIG. 14: (Color online) As Fig. 8 but for the negative-parity bands. The observed bands 5-7 are compared with the negative-parity configurations at close to prolate shape, $\gamma \approx 0$. The configuration labeled with a star has a neutron hole in the $[411]1/2$ orbital as illustrated in Fig. 15. In the upper panel, band 8 is also shown relative to the rotating liquid drop reference.

For the negative-parity bands, the comparison of signatures suggests instead that bands 5 and 6 stay close to prolate in their full spin range. The alignment at $I \approx 15$ may be explained as a standard paired crossing within the six $h_{11/2}$ neutrons (EF crossing, see Ref. [26]). Experiment and calculations are compared in Fig. 14 where the difference between experiment and calculations is more or less as expected considering that pairing is neglected in the CNS approach. The differences are similar to those at prolate shape, see Fig. 8, but they appear somewhat large for low spin states. This suggests that other shapes than those at $\gamma \approx 0^\circ$ might play a role for the low-spin states.

The fact that the energy as a function of spin for band

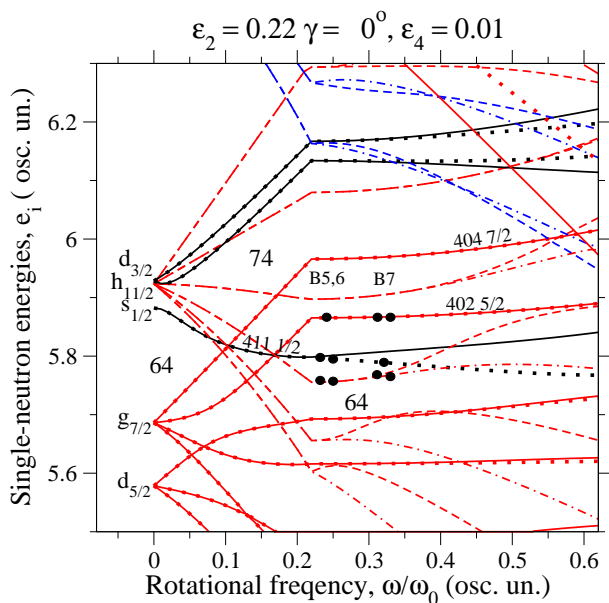


FIG. 15: (Color online) Single-neutron routhians at $\varepsilon_2 = 0.22$, $\gamma = 0^\circ$, $\varepsilon_4 = 0.01$. The suggested filling of orbitals above the small gap at $N = 64$ is illustrated for bands 5, 6, and 7.

7 (see Fig. 14) is similar to that of bands 5 and 6 suggests that it should be assigned to a similar configuration. However, because of the large signature splitting for the lowest $\mathcal{N}=5$ proton orbital, the bands with signature $\alpha = 1/2$ for these protons are calculated at a considerably higher energy, see Fig. 12. Instead, one may look for low-lying bands by shifting the orbital of the odd $\mathcal{N}=4$ neutron. The single-neutron orbitals at prolate deformation are displayed in Fig. 15 and the filling of the orbitals in bands 5 and 6 is illustrated, i.e., the odd neutron is located in the $[402]5/2$ orbital. Similar bands can be formed if this odd neutron is moved to either $[404]7/2$ or $[411]1/2$ where, however, the excitation energy of the corresponding bands becomes higher than observed for band 7. On the other hand, a small change of the single-particle parameters would shift the relative position of the j -shells. Thus, it would be straightforward to decrease the energy difference of the $[402]5/2$ and $[411]1/2$ orbitals whereas the energy difference between the $[402]5/2$ and $[404]7/2$ orbitals is less sensitive to parameter changes because both of these orbitals have

dominating or large amplitudes in the $g_{7/2}$ shell. Second, with the odd neutron in the $[404]7/2$ orbital, two signature degenerate bands would be formed while the signature splitting in the $[411]1/2$ orbital will lead to two bands with an appreciable signature splitting. This is in agreement with experiment where no signature degenerate partner of band 7 is observed. Based on these arguments, it is suggested that band 7 is formed with the odd neutron in the $[411]1/2$ orbital as illustrated in Fig. 15. Experiment and calculations are compared in Fig. 14, where, as anticipated above, the energy distance between bands 5, 6 and band 7 is too large in the calculations with present parameters. Considering the pseudo-spin partners $d_{5/2}g_{7/2}$ (dg) and $s_{1/2}d_{3/2}$ (sd), as done, e.g., in Ref. [35], the present interpretation means that bands 5,6 have three dg holes and two neutrons in sd orbitals while band 7 has two dg holes and one neutron in sd orbitals.

Band 8 has a somewhat different energy vs. spin dependence compared with bands 5-7, see Fig. 14. However, its behavior at low spin values and the observed links to band 6 indicate that it has a similar configuration as the other negative-parity bands. The shape of the energy vs. spin curve in Fig. 14 shows some similarities with the $[41-, 7+6]$ configuration, both at $\gamma \approx 35^\circ$ and $\gamma \approx -40^\circ$, see Fig. 12. It could have the odd neutron in the sd orbitals as suggested in Ref. [26].

C. Band termination

The level scheme of ^{124}Cs shows branchings at higher spin consisting of one to three transitions in a branch, see Fig 1. These energy levels may belong to non-collective excitations, as predicted by the CNS calculations (see above). The fact that bands 2 and 8 are irregular and clearly down-sloping at the highest spin values suggest that they have a small collectivity, possibly approach-

ing some favored termination. Band 2 is assigned to the $[41_-, 7_+, 6]$ configuration. In this configuration, several non-collective oblate states are calculated lower in energy than the collective branch assigned to band 2. It seems likely that these oblate states could explain the staggering observed at high spin in band 2. However, there is no calculated state which can explain the details, e.g. the relatively low energy of the 32^+ state. For the highest spin values in band 8, the configuration is even more uncertain, as concluded above

A more interesting feature are the branchings at high spin in bands 5 and 6. The 29^- state of band 5 is fed by a branch consisting of two transitions of energies 1338 and 1320 keV, and another γ ray of 1388 keV which corresponds to a smooth continuation of the collective band. In band 6, the 30^- state is fed by a 1203-keV transition. Stretched E2 character has been assumed for these transitions if multipolarity could not be determined. In the following, some of these non-collective states, which might belong to maximally aligned states of a configuration, are compared with the results of CNS calculations.

The relative energies, $E - E_{rld}$, for side branches and a few other bands are displayed in Fig. 16. The downslopes at high spin for the 5B and 6B branches are a strong indication that these states approach or reach termination. Comparing with calculations, the assignment of bands 5 and 6 above the band crossing at $I \approx 18$ as $[41,76]$ appears well established. With six neutrons in $h_{11/2}$ orbitals, the valence space of ^{124}Cs can be compared with that of ^{158}Er [43], the first example of band termination in heavy nuclei. In this nucleus, for $Z = 68$, a collective band with six protons in $h_{11/2}$ orbitals is crossed by a band with four protons in $h_{11/2}$ levels, where the latter band terminates at $I = 46$ as first predicted in [42] and then observed in experiment, see Ref. [43] and references therein. This terminating band is also discussed in Ref. [44], see, e.g., Fig. 12.11. In a similar way as for ^{158}Er ,

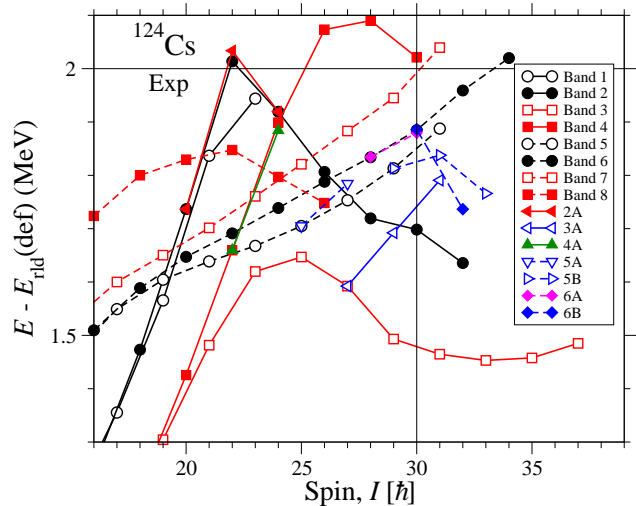


FIG. 16: (Color online) Observed energies relative to a rotating liquid drop energy for selected bands in ^{124}Cs . The states are selected to show the yrast line and possible band terminations. Positive-parity states are drawn by solid lines and negative-parity states by dashed lines.

the $\nu(h_{11/2})^6$ bands in ^{124}Cs are crossed by $\nu(h_{11/2})^4$ bands which terminate as

$$\pi[(dg)_{10}^4(h_{11/2})_{5.5}^1]_{15.5}\nu[(sd)_{0.5,1.5}^1(h_{11/2})_{16}^4]_{16.5,17.5}$$

with $I_{max} = 32, 33$. The $I_{max} = 33$ state is illustrated in a sloping Fermi surface diagram in Fig. 17.

Experiment and calculations are compared in Fig. 18. With the interpretation discussed above, the crossing between the $\nu(h_{11/2})^6$ and $\nu(h_{11/2})^4$ bands is reproduced by the calculations where both of the I_{max} states are observed. On the other hand, these I_{max} states are considerably more favored in experiment than in the calculations. Note also that non-collective states, e.g. with $I_{max} - 4$, are formed with one dg proton spin vector anti-aligned as illustrated in Fig. 17. These states are not observed here, contrary to ^{158}Er where an $I = 40$ state is observed with one anti-aligned hf neutron, see Fig. 12.9 of Ref. [44].

From comparisons with the $Z \approx 68$ region, terminations of the type observed here in $N \approx 68$ nuclei, were pre-

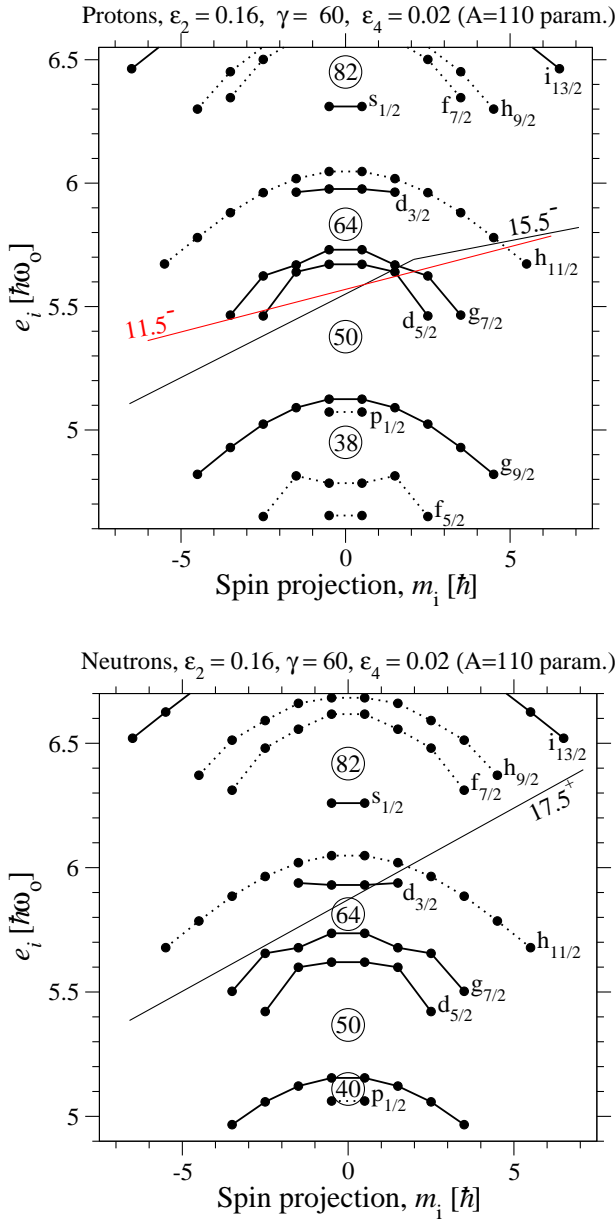


FIG. 17: (Color online) Sloping Fermi surface diagrams to illustrate how the $I_{max} = 33$ state in the $[41,54]$ configuration is built and how an aligned $I = 29$ can be built with one anti-aligned dg proton.

dicted long ago, e.g. in Ref. [33]. The fact that there is no other reasonable explanation for the observed down-sloping branches in the $E - E_{rld}$ plots is one reason why the present interpretation appears convincing.

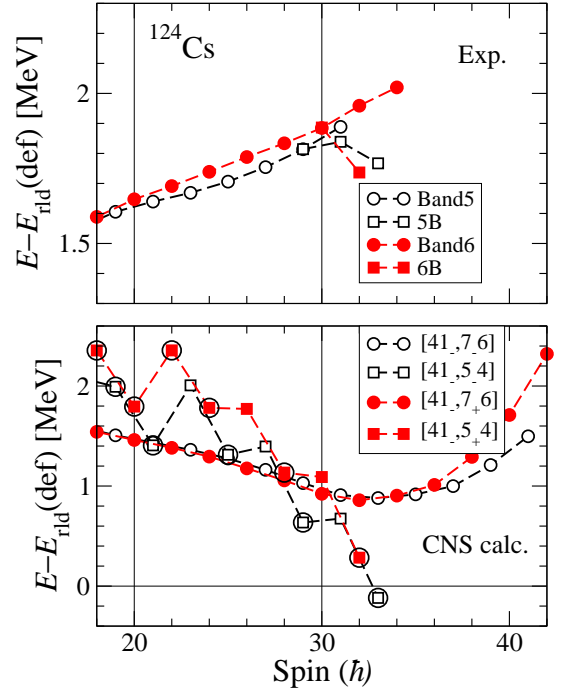


FIG. 18: (Color online) Comparison between experiment and calculations with the present interpretation of bands 5 and 6 and the high-spin branchings.

V. SUMMARY

High-spin structures of ^{124}Cs have been studied using the Gammasphere spectrometer. All previously known positive- and negative-parity states have been extended to higher spins. The low-spin states of the positive-parity bands were explained previously by a triaxial shape of the nucleus where chiral rotation is the favored excitation mode [14]. Band crossings have been observed in both pairs of chiral bands, bands 1-2 and 3-4, at $\hbar\omega \simeq 0.52\text{MeV}$. This is the first case where such band crossings have been observed in the side partner bands of odd-odd Cs nuclei. With the similar alignment gain of $i \sim 8\hbar$ in both these pairs, one can infer similar configurations for the bands.

The configurations of the bands have been explored within the framework of the CNS approach. The calculations suggest that the nuclear shape becomes prolate above spin $I = 22$ and the angular momentum gain in

the band crossing region, $I=20-28$, is due to contributions of several orbitals of valence shells, suggesting the absence of a paired band crossing in the positive-parity bands. Four signatures of the $\pi h_{11/2} \otimes \nu h_{11/2}^5$ configuration, i.e. the [41,65] configuration, have been assigned to the positive-parity bands 1-4. For the negative-parity bands, configurations [41,76] have been assigned to bands 5-7. The band crossings observed in the negative-parity bands are consistent with the alignment of a pair of neutrons from $h_{11/2}$ orbitals with an alignment gain of $5 \hbar$.

The calculations predict favored non-collective states between spin $I \sim 30-36$. The branches 5B and 6B agree well with the calculated results, suggesting that the highest spin states observed in these branches, $I=32,33$, corresponds to a favored termination at maximal spin in the $\pi(h_{11/2})^1\nu(h_{11/2})^4$ configuration. Furthermore, band 3 is only two transitions short of a smooth unfavored ter-

mination according to the CNS calculations. Thus, in a dedicated experiment it should be possible to observe both favored and unfavored terminations in the same nucleus.

VI. ACKNOWLEDGMENTS

We wish to thank the staff of the Berkeley Cyclotron for providing the beams and we greatly appreciate the support obtained from A.O. Machiavelli and the staff involved in running the Gammasphere spectrometer. The work was supported by MHRD, Government of India, BMBF (Germany) under the Contract No. 06 BN 907 and by DFG under Contract No. HU 325/10, Danish Natural Science Research Council, the Swedish Science Research Council, and the U. S. Department of Energy under Contract No. DE-AC02-05CH11231.

-
- [1] A. Grandierath, P. F. Mantica, R. Bengtsson, R. Wyss, P. von Brentano, A. Gelberg, and F. Seiffert, Nucl. Phys. A **597**, 427 (1996).
 - [2] R. Wyss *et al.*, Nucl. Phys. A **505**, 337 (1989).
 - [3] A. K. Singh *et al.*, Phys. Rev. C **70**, 034315 (2004).
 - [4] A. Al-Khatib *et al.*, Phys. Rev. C **74**, 014305 (2006).
 - [5] A. Al-Khatib *et al.*, Eur. Phys. J. A **36**, 21 (2008).
 - [6] Somnath Nag *et al.*, Phys. Rev. C **90**, 037302 (2014).
 - [7] Somnath Nag *et al.*, Phys. Rev. C **88**, 044335 (2013).
 - [8] Purnima Singh *et al.*, Phys. Rev. C **85**, 034319 (2012).
 - [9] Purnima Singh *et al.*, Phys. Rev. C **82**, 034301 (2010).
 - [10] Purnima Singh *et al.*, Phys. Rev. C **85**, 054311 (2012).
 - [11] A. Al-Khatib *et al.*, Phys. Rev. C **83**, 024306 (2011).
 - [12] T. Komatsubara *et al.*, Nucl. Phys. A **557**, 419c (1993).
 - [13] N. Tajima, Nucl. Phys. A **572**, 365 (1994).
 - [14] K. Selvakumar *et al.*, Phys. Rev. C **92**, 064307 (2015).
 - [15] U. Yong-Nam *et al.*, J. Phys. G **31**, B1 (2005).
 - [16] Shouyu Wang, Yunzuo Liu, T. Komatsubara, Yingjun Ma, and Yuhu Zhang, Phys. Rev. C **74**, 017302 (2006).
 - [17] T. Koike, K. Starota, C. J. Chiara, D. B. Fossan, and D. R. LaFosse, Phys. Rev. C **63**, 061304(R) (2001).
 - [18] K. Starosta *et al.*, Phys. Rev. Lett. **86**, 971 (2001).
 - [19] G. Rainovski *et al.*, Phys. Rev. C **68**, 024318 (2003).
 - [20] B. Qi, S. Q. Zhang, S. Y. Wang, J. M. Yao, and J. Meng, Phys. Rev. C **79**, 041302(R) (2009).
 - [21] A. V. Afanasjev and I. Ragnarsson, Nucl. Phys. A **608**, 176 (1996).
 - [22] T. Bengtsson and I. Ragnarsson, Nucl. Phys. A **436**, 14 (1985).
 - [23] B. G. Carlsson and I. Ragnarsson, Phys. Rev. C **74**, 011302 (2006).
 - [24] I. Y. Lee, Nucl. Phys. A **520**, 641c (1990).
 - [25] D. C. Radford, Nucl. Instrum. Methods Phys. Res. A **361**, 297 (1995).
 - [26] A. Gizon *et al.*, Nucl. Phys. A **694**, 63 (2001).
 - [27] T. Komatsubara *et al.*, Z. Phys. **A335**, 113 (1990).
 - [28] Jingbin Lu *et al.*, Phys. Rev. C **62**, 057304 (2000).
 - [29] Yang dong *et al.*, Chin. Phys. Lett. **26**, 082101 (2009).
 - [30] A. V. Afanasjev, D. B. Fossan, G. J. Lane, and I. Ragnarsson, Phys. Rep. **322**, 1 (1999).
 - [31] K. Pomorski and J. Dudek, Phys. Rev. C **67**, 044316 (2003).
 - [32] A. Schmidt *et al.*, Eur. Phys. J. A **2**, 21 (1998).
 - [33] I. Ragnarsson, Z. Xing, T. Bengtsson and M.A. Riley, Phys. Scr. **34**, 651 (1986).
 - [34] S. Y. Wang, B. Qi, and D. P. Sun, Phys. Rev. C **82**, 027303 (2010).
 - [35] Hai-Liang Ma, B.G. Carlsson, I. Ragnarsson, and H. Ryde Phys. Rev. C **90**, 014316 (2014).
 - [36] C. M. Petrache, I. Ragnarsson, Hai-Liang Ma, R. Leguillon, T. Zerrouki, D. Bazzacco, and S. Lunardi Phys. Rev. C **91**, 024302 (2015).
 - [37] F.S. Stephens, Rev. Mod. Phys. **47**, 43 (1975).
 - [38] J. Meyer-ter-Vehn, Nucl. Phys. A **249**, 111 (1975).
 - [39] G. Andersson *et al.*, Nucl. Phys. A **268**, 205 (1976).
 - [40] F. Dönau and S. Frauendorf, in *Proceedings of the Conference on High Angular Momentum Properties of Nuclei* (Oak Ridge, 1982), edited by N. R. Johnson (Harwood Academic, New York, 1983), p. 143.
 - [41] F. Dönau, Nucl. Phys. A **471**, 469 (1987).

- [42] T. Bengtsson and I. Ragnarsson, *Physica Scripta* **T5**, 165 (1983).
 [43] J. Simpson *et al.*, *Phys. Lett. B* **327**, 187 (1994).

- [44] *Shapes and Shells in Nuclear Structure*, S.G. Nilsson and I. Ragnarsson, Cambridge University Press, 1995.

TABLE I: Gamma-ray energies, level energies, angular distribution ratios, multipolarities, and spin assignments of γ -ray transitions of ^{124}Cs

Energy E_γ^a (keV)	Initial level energy E_i (keV)	Spin Assignment		Intensity ratio R_θ	Multipolarity Assignment
		J_i^π	$\rightarrow J_f^\pi$		
108.6	758	8^-	$\rightarrow 7^-$		
123.9	744	10^+	$\rightarrow 9^+$		
216.5	974	9^-	$\rightarrow 8^-$	0.64(4)	M1/E2
219.6	1275	12^+	$\rightarrow 11^+$	0.59(2)	M1/E2
222.4	1196	10^-	$\rightarrow 9^-$	0.60(4)	M1/E2
261.4	1892	13^+	$\rightarrow 12^+$		
298.3	1495	11^-	$\rightarrow 10^-$	0.65(3)	M1/E2
310.7	1805	12^-	$\rightarrow 11^-$	0.54(4)	M1/E2
311.8	1056	11^+	$\rightarrow 10^+$	0.57(2)	M1/E2
316.1	1988	14^+	$\rightarrow 13^+$	0.49(6)	M1/E2
325.1	974	9^-	$\rightarrow 7^-$		
334.3	1092	(9^-)	$\rightarrow 8^-$		
348.0	1092	(9^-)	$\rightarrow (7^-)$		
363.8	2169	13^-	$\rightarrow 12^-$	0.57(3)	M1/E2
370.3 ^c	1630	12^+	$\rightarrow 11^+$	0.64(5)	M1/E2
371.4	3039	–	$\rightarrow 14^+$		
372.1	2264	14^+	$\rightarrow 13^+$		
375.1	2544	14^-	$\rightarrow 13^-$		
397.1	1672	13^+	$\rightarrow 12^+$	0.58(3)	M1/E2
400.0	2944	15^-	$\rightarrow 14^-$	0.64(5)	M1/E2
401.2 ^c	2665	15^+	$\rightarrow 14^+$	0.69(3)	M1/E2
405.4	3350	16^-	$\rightarrow 15^-$	0.70(8)	M1/E2
412.1	974	9^-	$\rightarrow 8^+$		
415.0	1611	(11^-)	$\rightarrow 10^-$		
417.2	3767	17^-	$\rightarrow 16^-$	0.59(5)	M1/E2
435.6	4642	19^-	$\rightarrow 18^-$		
435.7	1056	11^+	$\rightarrow 9^+$	1.64(26)	E2
438.9	1196	10^-	$\rightarrow 8^-$	1.41(9)	E2
439.0	4206	18^-	$\rightarrow 17^-$	0.74(10)	M1/E2
453.7	5581	21^-	$\rightarrow 20^-$	0.64(6)	M1/E2
456.8	2445	15^+	$\rightarrow 14^+$	0.52(5)	M1/E2
457.3	2263	(13^-)	$\rightarrow 12^-$		
463.7	6550	23^+	$\rightarrow 22^+$	0.48(5)	M1/E2
483.2	3572	17^+	$\rightarrow 16^+$	0.57(9)	M1/E2
485.4	3343	17^+	$\rightarrow 16^+$	0.73(7)	M1/E2
492.6	1289	(10^-)	$\rightarrow (8^-)$		
506.0 ^c	2136	13^+	$\rightarrow 12^+$	0.32(4)	M1/E2
509.8	4341	19^+	$\rightarrow 18^+$	0.59(5)	M1/E2
516.2	1260	11^+	$\rightarrow 10^+$		
517.2	5422	21^+	$\rightarrow 20^+$	0.65(5)	M1/E2

Energy E_γ^a (keV)	Initial level energy E_i (keV)	Spin Assignment $J_i^\pi \rightarrow J_f^\pi$	Intensity ratio R_θ	Multipolarity Assignment
519.6	1611	$11^- \rightarrow 9^-$		
520.7	1495	$11^- \rightarrow 9^-$	1.21(7)	E2
531.4	1275	$12^+ \rightarrow 10^+$	1.39(8)	E2
531.5 ^c	2668	$14^+ \rightarrow 13^+$	0.71(4)	M1/E2
531.9	1289	$(10^-) \rightarrow 8^-$		
544.5	3412	$- \rightarrow 15^+$		
574.7 ^c	1630	$12^+ \rightarrow 11^+$	0.63(9)	M1/E2
576.5	1196	$10^- \rightarrow 9^+$		
591.5 ^c	2264	$14^+ \rightarrow 13^+$	0.54(8)	M1/E2
603.6	2867	$15^+ \rightarrow 14^+$		
609.0	1805	$12^- \rightarrow 10^-$	1.28(8)	E2
616.5	1892	$13^+ \rightarrow 12^+$		
616.7	1672	$13^+ \rightarrow 11^+$	1.21(8)	E2
631.7	1892	$13^+ \rightarrow 11^+$		
633.5	2264	$14^+ \rightarrow 12^+$		
644.1	3089	$16^+ \rightarrow 15^+$	0.69(3)	M1/E2
651.3	2263	$(13^-) \rightarrow (11^-)$	1.42(7)	E2
660.0	1949	$(12^-) \rightarrow (10^-)$		
674.5	2169	$13^- \rightarrow 11^-$	1.30(12)	E2
676.6	2665	$15^+ \rightarrow 14^+$		
713.2	1988	$14^+ \rightarrow 12^+$	1.34(8)	E2
738.9	2544	$14^- \rightarrow 12^-$	1.32(9)	E2
745.6	3008	$(15^-) \rightarrow (13^-)$	1.18(8)	E2
747.0	4090	$18^+ \rightarrow 17^+$		
749.8	1805	$12^- \rightarrow 11^+$		
750.9	1495	$11^- \rightarrow 10^+$		
753.0	1949	$(12^-) \rightarrow 10^-$		
761.3	2711	$(14^-) \rightarrow (12^-)$		
772.9	2445	$15^+ \rightarrow 13^+$	1.36(9)	E2
773.3	2665	$15^+ \rightarrow 13^+$		
775.1	2944	$15^- \rightarrow 13^-$	1.40(18)	E2
805.4	3350	$16^- \rightarrow 14^-$	1.45(6)	E2
808.6	3817	$(17^-) \rightarrow (15^-)$	1.39(10)	E2
810.5	4642	$19^- \rightarrow 18^+$		
822.6	3767	$17^- \rightarrow 15^-$	1.18(12)	E2
825.5	3089	$16^+ \rightarrow 14^+$		
853.0	3564	$(16^-) \rightarrow (14^-)$		
853.0	4417	$(18^-) \rightarrow (16^-)$		
856.2	4206	$18^- \rightarrow 16^-$	1.17(5)	E2
867.6	1611	$(11^-) \rightarrow 10^+$		
869.0	2857	$16^+ \rightarrow 14^+$	1.33(8)	E2
870.0	4687	$(19^-) \rightarrow (17^-)$	1.33(8)	E2
872.0	2544	$14^- \rightarrow 13^+$		
874.6	4642	$19^- \rightarrow 17^-$	1.22(12)	E2
875.0	5216	$20^+ \rightarrow 19^+$		
892.5	5309	$(20^-) \rightarrow (18^-)$		
894.0	2169	$13^- \rightarrow 12^+$		
897.6	3343	$17^+ \rightarrow 15^+$	1.22(8)	E2
904.5	3350	$16^- \rightarrow 15^+$		
907.5	3572	$17^+ \rightarrow 15^+$	1.46(19)	E2
909.5	3767	$17^- \rightarrow 16^+$		

Energy E_γ^a (keV)	Initial level energy E_i (keV)	Spin Assignment $J_i^\pi \rightarrow J_f^\pi$	Intensity ratio R_θ	Multipolarity Assignment
916.0	7376	$24^+ \rightarrow 22^+$	1.48(18)	E2
921.3	5127	$20^- \rightarrow 18^-$	1.52(18)	E2
936.5	7376	$24^+ \rightarrow 22^+$	1.30(12)	E2
939.4	5581	$21^- \rightarrow 19^-$	1.18(9)	E2
955.5	5642	$(21^-) \rightarrow (19^-)$	1.38(4)	E2
955.9	2944	$15^- \rightarrow 14^+$		
965.0	6274	$(22^-) \rightarrow (20^-)$		
973.6	3831	$18^+ \rightarrow 16^+$	1.25(8)	E2
980.0	7254	$(24^-) \rightarrow (22^-)$		
987.5	2263	$(13^-) \rightarrow 12^-$		
990.0	9931	$- \rightarrow 27^-$		
991.4	6119	$22^- \rightarrow 20^-$	1.16(12)	E2
998.0	4341	$19^+ \rightarrow 17^+$	1.28(9)	E2
1000.5 ^b	4090	$18^+ \rightarrow 16^+$	1.27(9)	E2
1000.5 ^b	8376	$26^+ \rightarrow 24^+$		
1016.8	6439	$22^+ \rightarrow 21^+$		
1017.6	6598	$23^- \rightarrow 21^-$	1.35(18)	E2
1029.5	4602	$19^+ \rightarrow 17^+$	1.14(15)	E2
1037.3	6460	$22^+ \rightarrow 21^+$		
1047.7	6690	$(23^-) \rightarrow (21^-)$	1.59(24)	E2
1064.5	8318.7	$(26^-) \rightarrow (24^-)$		
1074.3	4905	$20^+ \rightarrow 18^+$	1.42(13)	E2
1078.4	7197	$24^- \rightarrow 22^-$	1.23(12)	E2
1081.7	5422	$21^+ \rightarrow 19^+$	1.38(12)	E2
1086.5	11017	$- \rightarrow -$		
1096.0	6874	$(23^+) \rightarrow 21^+$		
1098.6 ^b	8747	$27^+ \rightarrow 25^+$	1.49(12)	E2
1098.6 ^b	7648	$25^+ \rightarrow 23^+$		E2
1107.1	9483	$28^+ \rightarrow 26^+$	1.20(10)	E2
1109.1	7708	$25^- \rightarrow 23^-$	1.23(9)	E2
1126.0	5216	$20^+ \rightarrow 18^+$	1.29(16)	E2
1127.1	6550	$23^+ \rightarrow 21^+$	1.22(10)	E2
1132.3	7822	$(25^-) \rightarrow (23^-)$	1.10(12)	E2
1134.6	9881	$29^+ \rightarrow 27^+$	1.22(10)	E2
1162.1	8359	$26^- \rightarrow 24^-$	1.29(12)	E2
1170.7	8512	$- \rightarrow 24^+$		
1175.8	5778	$21^+ \rightarrow 19^+$	1.26(18)	E2
1180.6	6086	$22^+ \rightarrow 20^+$	1.21(12)	E2
1201.5	8909	$27^- \rightarrow 25^-$	1.29(10)	E2
1203.0	12127	$(32^-) \rightarrow 30^-$		
1205.3	11060	$(30^+) \rightarrow (28^+)$		
1211.4	9855	$(28^+) \rightarrow 26^+$		
1216.4	9039	$(27^-) \rightarrow (25^-)$	1.33(15)	E2
1223.5	6439	$22^+ \rightarrow 20^+$	1.32(16)	E2
1233.1	8941	$27^- \rightarrow 25^-$	1.17(11)	E2
1240.1	9599	$28^- \rightarrow 26^-$	1.42(18)	E2
1244.0	6460	$22^+ \rightarrow 20^+$	1.26(18)	E2
1252.6	12026	$32^+ \rightarrow 30^+$		
1255.0	7341	$24^+ \rightarrow 22^+$	1.17(17)	E2
1270.4	7356	$24^+ \rightarrow 22^+$	1.18(18)	E2
1284.7	11166	$31^+ \rightarrow 29^+$	1.13(18)	E2

Energy E_γ^a (keV)	Initial level energy E_i (keV)	Spin Assignment $J_i^\pi \rightarrow J_f^\pi$	Intensity ratio R_θ	Multipolarity Assignment
1287.1	8643	$26^+ \rightarrow 24^+$	1.10(18)	E2
1289.6	10773	$30^+ \rightarrow 28^+$	1.22(17)	E2
1294.5	10204	$29^- \rightarrow 27^-$	1.35(19)	E2
1296.3	10335	$(29^-) \rightarrow (27^-)$	1.41(18)	E2
1319.0	10918	$(30^-) \rightarrow 28^-$		
1320.2	12862	$(33^-) \rightarrow 31^-$		
1325.0	10924	$30^- \rightarrow 28^-$	1.20(16)	E2
1334.0	10081	$29^+ \rightarrow 27^+$	1.24(16)	E2
1338.0	11542	$31^- \rightarrow 29^-$	1.15(12)	E2
1379.6	12546	$33^+ \rightarrow 31^+$	1.26(20)	E2
1388.0	11592	$(31^-) \rightarrow 29^-$		
1408.1	11743	$(31^-) \rightarrow (29^-)$		
1412.5	11493	$31^+ \rightarrow 29^+$	1.26(13)	E2
1427.2	12351	$(32^-) \rightarrow 30^-$		
1472.7	14018	$(35^+) \rightarrow 33^+$	1.25(22)	E2
1482.4	14028	$- \rightarrow 33^+$		
1491.0	13842	$(34^-) \rightarrow (32^-)$		
1571.0	15589	$(37^+) \rightarrow (35^+)$		

^a The uncertainties are between 0.2 and 1.0 keV depending on intensity

^b Measurement of angular distribution ratio (R_θ) was not possible due to presence of γ rays of overlapping energy

^c The angular distribution ratio (R_θ) has been determined from gated spectrum on dipole transition
